Anomalous physical properties of Heusler-type $Co_2Cr(Ga,Si)$ alloys and thermodynamic study on reentrant martensitic transformation

Xiao Xu,[1,*] Makoto Nagasako,[2] Mitsuo Kataoka,[3] Rie Y. Umetsu,[2] Toshihiro Omori,[1] Takeshi Kanomata,[1,4] and Ryosuke Kainuma[1]

[1]*Department of Materials Science, Tohoku University, Sendai 980-8579, Japan*
[2]*Institute for Materials Research, Tohoku University, Sendai 980-8577, Japan*
[3]*Laboratory for Solid State Physics, Moniwadai 2-1-1, Taihaku-ku, Sendai 982-0252, Japan*
[4]*Research Institute for Engineering and Technology, Tohoku Gakuin University, Tagajo 985-8537, Japan*

(Received 26 December 2014; revised manuscript received 1 March 2015; published 31 March 2015)

Electronic, magnetic, and thermodynamic properties of $Co_2Cr(Ga,Si)$-based shape-memory alloys, which exhibit reentrant martensitic transformation (RMT) behavior, were studied experimentally. For electric resistivity (ER), an inverse (semiconductor-like) temperature dependence in the parent phase was found, along with anomalous behavior below its Curie temperature. A pseudobinary phase diagram was determined, which gives a "martensite loop" clearly showing the reentrant behavior. Differential scanning calorimetry and specific-heat measurements were used to derive the entropy change ΔS between martensite and parent phases. The temperature dependence of the derived ΔS was analyzed thermodynamically to confirm the appearances of both the RMT and normal martensitic transformation. Detailed studies on the specific heat in martensite and parent phases at low temperatures were also conducted.

DOI: 10.1103/PhysRevB.91.104434 PACS number(s): 81.30.Kf, 62.20.fg, 72.15.Cz, 75.40.−s

I. INTRODUCTION

Generally, during conventional martensitic transformation (MT), the parent (P) phase is stable at high temperatures, and the martensite (M) phase is formed during cooling. Conventional shape-memory alloys (SMA) show the shape-memory effect (SME) during reverse MT, and therefore, only heating realizes SME. Very recently, we have reported unusual MT in $Co_2Cr(Ga,Si)$ Heusler alloys [1]. In $Co_2Cr(Ga,Si)$ alloys, the high-temperature P phase ($L2_1$, bcc) transforms to the M phase ($D0_{22}$, fct) at an intermediate temperature, and the M phase transforms back to the P phase ($L2_1$, bcc) at low temperatures, showing reentrant martensitic transformation (RMT) behavior. Moreover, while heating a deformed sample from the M phase results in conventional SME, cooling the sample brings out a cooling-induced SME. The occurrence of these novel phenomena originates from the reversal of phase stability between P and M phases. However, neither direct experimental evidence nor thermodynamic derivation has been obtained. In this study, we systematically investigate the physical properties and magnetic phase diagrams in the $Co_2Cr(Ga,Si)$ alloy system. Several anomalous properties were found, which are considered to be closely related to the novel physical phenomena reported in our previous study [1].

II. EXPERIMENTAL PROCEDURES

$Co_xCr_{78-x}Ga_{11}Si_{11}$(Co$x$, $x = 48.7$, 49.7, 50.4, 50.8, 51.1, 51.3, 51.6, 51.7, 52.3, 53.1, 53.5, 53.8, 54.2, 54.9) alloys were prepared by induction melting in an Ar atmosphere. Solution treatment were conducted at 1373 K for 24 h followed by water-quenching. Composition analyses were conducted using an electron probe microanalyzer (EPMA). Electronic resistivity (ER) measurements were performed using the four-probe method, where ac currents in the temperature range from 2 to 390 K at 2 K/min and dc currents in the temperature range of 300 to 773 K at 5 K/min were used. Specific-heat measurements from 1.9 to 200 K were conducted with the relaxation method using a physical properties measurement system (PPMS). Specific-heat measurements from 90 to 670 K were conducted with the heat-flow method using a differential scanning calorimeter (DSC) calibrated by a standard sapphire sample according to DIN 51007 at 10 K/min. Thermoanalysis was carried out using a DSC at 10 K/min. Thermomagnetization measurements were conducted using a superconducting quantum interference device magnetometer of a magnetic property measurement system (MPMS) and the ac magnetic susceptibility (ACMS) option of the PPMS at 2 K/min.

III. EXPERIMENTAL RESULTS AND DISCUSSION

A. Electric transport properties

Figure 1(a) shows the temperature dependence of the ER for Cox alloys. The measurement sequences are indicated by the numbered arrows. For Co54.2, only the M phase was found below RT, where the ER decreases with decreasing temperature, showing a normal metallic behavior. For Co51.7, as previously reported [1], the RMT was observed below room temperature (RT), and when the alloy was heated up to high temperatures the normal reverse MT was also detected. However, when the alloy was heated up to high temperatures with a low heating rate, diffusion due to the atomic ordering may have occurred, resulting in the stabilization of the P phase and suppression of the MT. Therefore, only the Curie temperature of the P phase $T_{C,P}$ was detected during cooling. For Co49.7, only $T_{C,P}$ was detected. The slight increase in ER below 50 K may be caused by impurities.

Closer examination reveals several characteristic transport properties of $Co_2Cr(Ga,Si)$ alloys. (1) The ER of the P phase

*Corresponding author: xu@material.tohoku.ac.jp

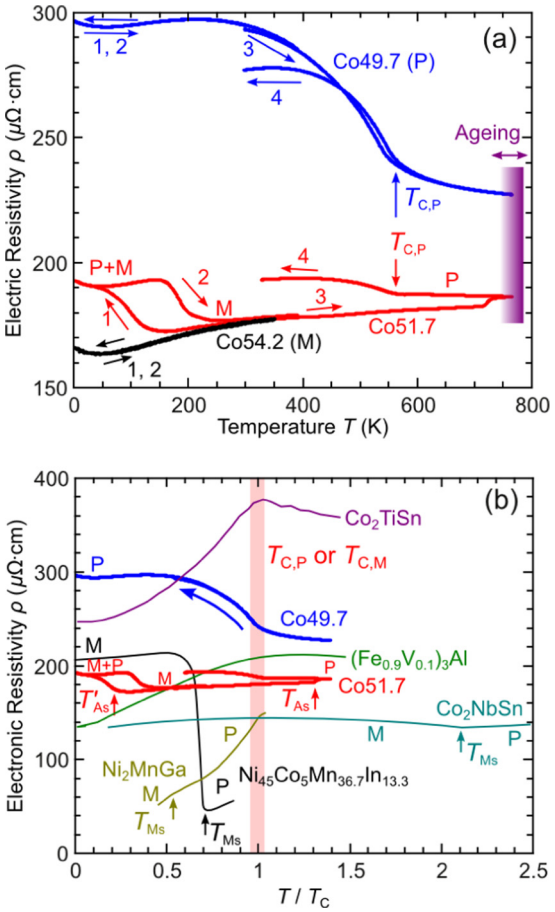

FIG. 1. (Color online) (a) Electric resistivity vs temperature for $Co_xCr_{78-x}Ga_{11}Si_{11}$ (Cox) alloys. For Co51.7, normal and reentrant martensitic transformations (RMT) were observed. $T_{C,P}$ indicates the Curie temperature of the parent phase. (b) The electronic resistivities of Co49.7 and Co51.7 compared with those of Ni_2MnGa [2], $Ni_{45}Co_5Mn_{36.7}In_{13.3}$ [3], $(Fe_{0.9}V_{0.1})_3Al$ [4], Co_2TiSn [5], and Co_2NbSn [6]. The temperatures for the alloys except for Co_2NbSn are normalized against each alloy's $T_{C,P}$s, while that for Co_2NbSn is normalized against its Curie temperature of martensite phase $T_{C,M}$.

is greater than that of the M phase, with a large difference. (2) Although having normal values as a metal, the ER of the P phase increases with decreasing temperature, showing an inverse temperature (semiconductor-like) dependence. (3) The ER of the P phase bends upward below $T_{C,P}$, showing stronger inverse temperature dependence.

Item (1) originates from the drastic change of crystal structure, such as in Fe-Ni alloys [7]. However, $Co_2Cr(Ga,Si)$ alloys behave differently than other ferromagnetic [8] and metamagnetic [9] shape-memory alloys. For conventional magnetic shape-memory alloys [8,9], the electronic transport properties also show abrupt changes during the first-order martensitic transformation. As a representative of the ferromagnetic shape-memory alloys (FMSMA), Ni_2MnGa shows a discontinuous increase in the ER of about 0.5%–9% during the transformation into martensite phase [2]. The residual resistivity (RR) is very small, i.e., several tens of $\mu\Omega$ cm [2]. On the other hand, for metamagnetic shape-memory alloys (MMSMA) such as the Ni-(Co)-Mn-In alloy, the ER of the martensite phase is almost 10 times larger than that of the parent phase, with RR of more than 200 $\mu\Omega$ cm [3,10]. Cox alloys also show a large difference in ER between P and M phases; however, the P phase has a larger value of ER, and RR of the P phase is more than 300 $\mu\Omega$ cm. The behavior in item (2) can be generally found for semiconductors and for metallic alloys with high ER values at RT [11]. However, for item (3), although similar behavior has been observed for some alloys at the Néel temperature which are antiferromagnetic [12], it is a very unique behavior unknown for other ferromagnetic Heusler alloys.

Figure 1(b) shows a comparison of the temperature dependence of ER for several ferromagnetic Heusler alloys, where the temperature of each alloy is normalized against its own Curie temperatures. For conventional alloys such as Ni_2MnGa [2], a typical temperature dependence of ER is observed throughout the wide temperature range. The small downward bending of ER around $T_{C,P}$ is attributed to the

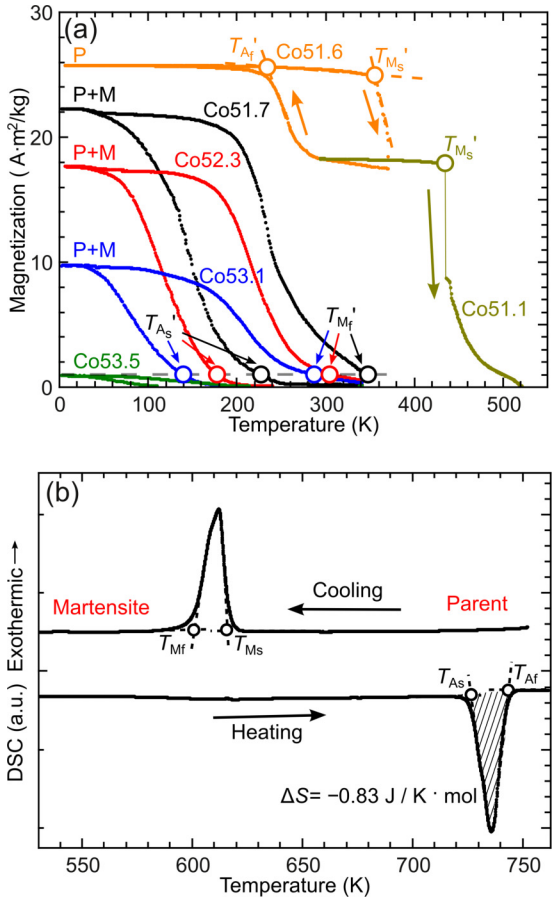

FIG. 2. (Color online) (a) Thermomagnetization measurements for Co51.1 to Co53.5 alloys under 500 Oe. For RMT, forward transformation starting (T_{M_s}') and finishing (T_{M_f}') temperatures and reverse transformation starting (T_{A_s}') and finishing (T_{A_f}') temperatures are indicated. (b) Thermoanalysis of Co51.7 at high temperature using a differential scanning calorimeter. For MT, forward transformation starting (T_{M_s}) and finishing (T_{M_f}) temperatures and reverse transformation starting (T_{A_s}) and finishing (T_{A_f}) temperatures are indicated. Moreover, the transformation entropy change during the martensitic transformation ΔS was determined by estimating the hatched area.

TABLE I. Composition, apparent Debye temperature $\theta_{D,i}$, electronic specific-heat coefficient γ_i, Curie temperature of the parent phase $T_{C,P}$, forward martensitic transformation starting (T_{M_s}) and finishing (T_{M_f}) temperatures, and reverse martensitic transformation starting (T_{A_s}) and finishing (T_{A_f}) temperatures (T_{A_s}', T_{A_f}', T_{M_s}', and T_{M_f}' for the reentrant transformation) of $Co_xCr_{78-x}Ga_{11}Si_{11}$ (Cox) alloys. A dash (-) means a value does not exist. Unmeasured values are left blank. Note that mol is defined here as Avogadro's number of a unit $Co_{0.01x}Cr_{(0.78-0.01x)}Ga_{0.11}Si_{0.11}$. The data of Co51.7 were taken from Ref. [1].

Alloy	Composition/%				Phase at ground state	$\theta_{D,i}$ (K)	γ_i (mJ mol^{-1} K^{-2})	Transformation temperatures (K)								
	Co	Cr	Ga	Si				T_{A_s}	T_{A_f}	T_{M_s}	T_{M_f}	T_{A_s}'	T_{A_f}'	T_{M_s}'	T_{M_f}'	$T_{C,P}$
Co48.7	48.7 ± 0.2	30.1 ± 0.2	10.5 ± 0.1	10.7 ± 0.2	P	495	4.17	–	–	–	–	–	–	–	–	540
Co49.7	49.7 ± 0.1	28.8 ± 0.2	11.2 ± 0.2	10.3 ± 0.2	P	444	4.45	–	–	–	–	–	–	–	–	537
Co50.4	50.4 ± 0.1	28.4 ± 0.2	10.4 ± 0.1	10.8 ± 0.2	P	418	4.65	–	–	–	–	–	–	–	–	
Co50.8	50.8 ± 0.2	27.9 ± 0.2	10.5 ± 0.1	10.8 ± 0.2	P			–	710	513	–	–	–	–	–	538
Co51.1	51.1 ± 0.2	27.7 ± 0.2	10.5 ± 0.1	10.7 ± 0.2	P			696	721	555	527	–	–	435	–	–
Co51.3	51.3 ± 0.2	27.4 ± 0.1	10.6 ± 0.1	10.7 ± 0.1	P	416	5.12	706	719	569	548					–
Co51.6	51.6 ± 0.2	27.2 ± 0.1	10.4 ± 0.1	10.8 ± 0.2	P							–	235	355	–	–
Co51.7	51.7 ± 0.1	26.8 ± 0.2	10.6 ± 0.1	10.9 ± 0.3	P+M	–	–	726	743	617	600	226	–	–	348	–
Co52.3	52.3 ± 0.2	26.4 ± 0.2	10.5 ± 0.1	10.8 ± 0.1	P+M	–	–	730	746	628	613	177	–	–	306	–
Co53.1	53.1 ± 0.1	25.9 ± 0.1	10.6 ± 0.1	10.4 ± 0.3	P+M	–	–	740	756	653	636	138	–	–	284	–
Co53.5	53.5 ± 0.3	25.1 ± 0.3	10.6 ± 0.1	10.8 ± 0.4	P+M	–	–	750	767	674	658	–	–	–	–	–
Co53.8	53.8 ± 0.3	24.8 ± 0.3	10.6 ± 0.1	10.8 ± 0.4	M	385	15.6					–	–	–	–	–
Co54.2	54.2 ± 0.2	24.4 ± 0.1	10.6 ± 0.1	10.8 ± 0.2	M	386	16.3	768	790	702	671	–	–	–	–	–
Co54.9	54.9 ± 0.2	23.7 ± 0.2	10.6 ± 0.2	10.8 ± 0.3	M	430	17.2					–	–	–	–	–

decrease of the spin-disorder scattering. Kasuya [13] and de Gennes and Friedel [14] have deduced a formula for spin-disorder resistivity using the free-electron model. Recently, some alloys, such as $(Fe_{0.9}V_{0.1})_3Al$ [4] and Co_2TiSn [5], have been reported to show a cusp near the Curie temperature and an inverse temperature dependence above the Curie temperature. This phenomenon has been explained by Kataoka by taking into account the role of spin fluctuation in ER of the *s-d* system [15]. Nevertheless, below the Curie temperature, all these formerly reported Heusler alloys show a normal temperature dependence of ER. Also, note that Co_2NbSn is another Co-based Heusler alloy showing martensitic transformation, but without reentrant behavior [16]. The ER of Co_2NbSn shows a slight inverse temperature dependence below the martensitic transformation temperature T_{M_s}; however, the behavior becomes normal below the Curie temperature inside the martensite [6]. Anyhow, the behavior of ER below the Curie temperature of the P phase in $Co_xCr_{78-x}Ga_{11}Si_{11}$ (Cox) cannot be explained by current theoretical understanding [13–15].

B. Determination of pseudobinary phase diagram

Figure 2(a) shows thermomagnetization curves for Co51.1 to Co53.5 alloys under 500 Oe. The RMT temperatures decrease with increasing Co content, as indicated by T_{M_s}', T_{M_f}', T_{A_s}', and T_{A_f}'. T_{M_s}' and T_{A_f}' were defined by extrapolation, while T_{A_s}' and T_{M_f}' were defined as the temperatures at 1 emu/g, because of the difficulty of extrapolation in the presence of partial transformations. Figure 2(b) shows the results of thermoanalysis by DSC for the Co51.7 alloy. Transformation temperatures T_{M_s}, T_{M_f}, T_{A_s}, and T_{A_f} for normal MT at high temperature were determined. The entropy change during martensitic transformation ΔS, which is defined by

$$\Delta S = S_M - S_P, \tag{1}$$

was also determined for normal MT. Samples with $x < 51$ do not show martensitic transformation. The transformation temperatures determined in Fig. 2 are listed in Table I with their compositions.

The data in Table I are plotted against Co content in Fig. 3, where $T_0 = (T_{M_s} + T_{A_f})/2$ or $T_0 = (T_{M_s}' + T_{A_f}')/2$ was used to estimate the thermodynamic equilibrium temperatures in Fig. 3(a) and $T_0' = (T_{A_s} + T_{M_f})/2$ or $T_0' = (T_{A_s}' + T_{M_f}')/2$ was used in Fig. 3(b). It is clearly seen that the RMT behavior appears in the concentration range around 51%–53%. Therefore, a "martensite loop" was observed in this phase diagram, which is similar to the "γ loop" in the Fe-Cr and Fe-Al binary phase diagrams. The magnetism of the M phase with no spontaneous magnetization is assumed to be paramagnetic by referring to the paramagnetic M phase in Ni-Mn-Sn ferromagnetic SMA [17].

Most Co-based Heusler alloys are half metals with a pseudogap at the Fermi level [18]. These alloys are generally considered to have excellent phase stability and are not likely to undergo martensitic transformation. Half-metallic behaviors have been reported for $Co_2Cr(Ga,Si)$ alloys by both calculation [19] and experiment [20]. Therefore, it is of great interest to understand why $Co_2Cr(Ga,Si)$ alloys show MT and RMT behaviors. We present a qualitative thermodynamic consideration based on experimental measurements by various methods in the next section.

C. Entropy and Gibbs energy changes during MT and RMT

Figure 4 shows specific heats of Co51.3 and Co53.8 in the temperature range of 2 to 200 K. It was found that the specific heat of Co53.8 in the M phase is larger than that of Co51.3 in the P phase at common temperatures. The entropy change by MT can be obtained by substituting

$$S_i = S_{0,i} + \int_0^T \frac{C_{P,i}}{T} dT \tag{2}$$

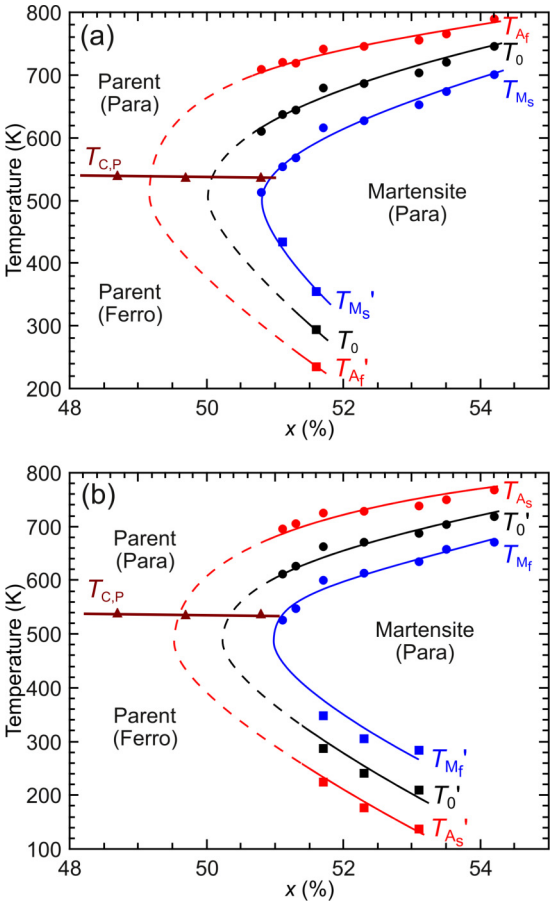

FIG. 3. (Color online) Magnetic phase diagram for Cox alloys. Refer to Fig. 2 for the definition of transformation temperatures. (a) $T_0 = (T_{M_s} + T_{A_f})/2$ or $T_0 = (T_{M_s}' + T_{A_f}')/2$ and (b) $T_0' = (T_{A_s} + T_{M_f})/2$ or $T_0' = (T_{A_s}' + T_{M_f}')/2$ were used to estimate the thermodynamic equilibrium temperatures T_0 and T_0'. Note that T_0 in (a) has a simpler physical meaning than T_0' in (b). This is because the equilibrium state of T_0' is referenced to the martensite phase, in which nonchemical elastic energy is included. However, they have a very similar shape, and there are more data for T_0' in the reentrant branch. Dashed and solid lines are visual guides. A clear "martensite loop" was found.

into Eq. (1). From now on, the subscript i for any physical quantity is used to represent the M or P phase. In Fig. 5(a), data in orange show ΔS estimated using Eqs. (1) and (2), where the experimental data for Co51.3 and Co53.8 shown in Fig. 4 were used. $\Delta S = 0$ at 0 K is assumed according to the third law of thermodynamics. The large error bars of the orange line originate from the fact that errors in the specific heats shown in Fig. 4 are about 2% of their raw data. Moreover, other experimental values of ΔS for some alloys of Cox are also plotted with allowance for small modifications of x around $x = 52.5$. Blue squares show ΔS calculated using the Clausius-Clapeyron equation [22] with data from compression tests for Co51.3 [1]. The red circle shows ΔS obtained from thermoanalyses using DSC for Co51.7, as shown in Fig. 2(b). Although the alloy compositions are not the same, it is clear that ΔS shows positive values at low temperatures but negative values at high temperatures. This trend is roughly represented

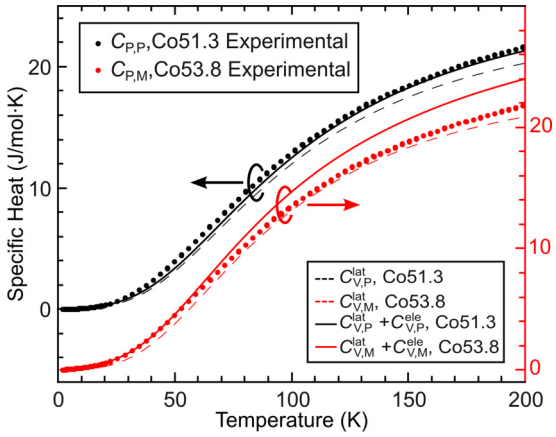

FIG. 4. (Color online) Experimentally measured specific heat between 2 and 200 K of Co51.3 and Co53.8 alloys. Solid and dashed lines show specific heat calculated using the Debye model for the lattice contribution $C_{V,i}^{lat}$ and $\gamma_i T$ for the electronic contribution $C_{V,i}^{ele}$ [21]. A large discrepancy between $C_{P,M}$ and $(C_{V,M}^{lat} + C_{V,M}^{ele})$ was found for Co53.8 in the martensite phase. Refer to Sec. III D for details.

by ΔS_{trend}. This is a unique and abnormal behavior because normal SMAs would not show a sign reversal of ΔS, as shown schematically for a nonmagnetic system by ΔS^{nonmag} in Fig. 5(a) [23]. The overall anomalous contribution to ΔS is schematically shown as ΔS^{anom}. As shown in the Appendix, a roughly estimated value of the magnetic contribution to

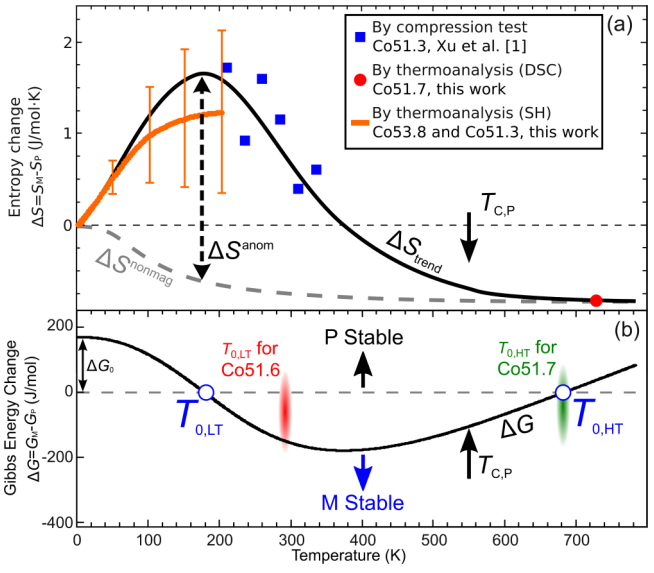

FIG. 5. (Color online) (a) Experimental values of the martensitic transformation entropy change ΔS. ΔS from compression tests [1] and thermoanalysis by DSC [see Fig. 2(b)] and specific heat (SH; see Fig. 4) are plotted. Large error bars on the orange line are attributed to the errors of 2% in the specific heats shown in Fig. 4. The black line shows the trend of experimental data. ΔS^{nonmag} schematically shows ΔS for a conventional shape-memory alloy without a magnetic contribution [23]. ΔS^{anom} indicates the anomalous contribution to ΔS. (b) Gibbs energy change ΔG estimated using the ΔS_{trend} curve in (a). Since ΔG intersects with the temperature axis twice, a reentrant behavior of martensitic transformation is qualitatively obtained.

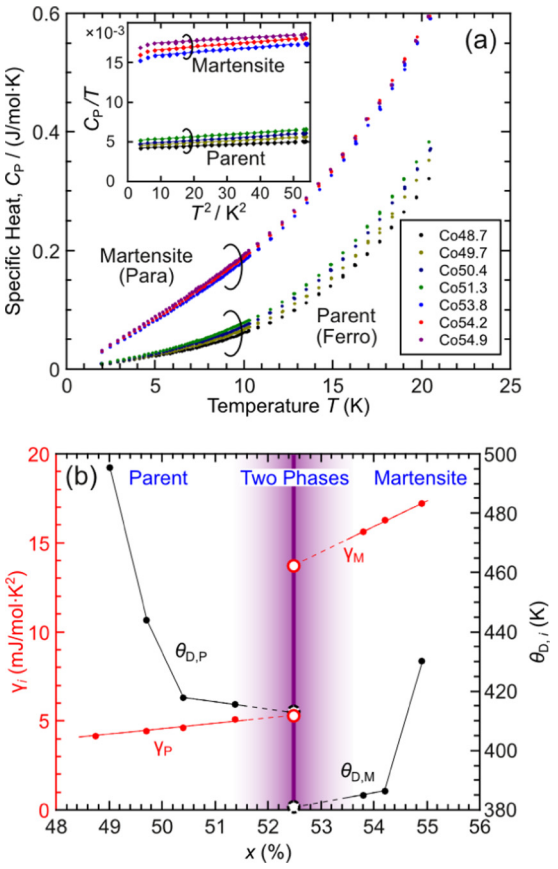

FIG. 6. (Color online) (a) Specific heat vs temperature in the temperature range of 1.9–20 K for $Co_xCr_{78-x}Ga_{11}Si_{11}$ (Cox) alloys and the C_P/T vs T^2 plot (inset). (b) Apparent Debye temperature $\theta_{D,i}$ and electronic specific-heat coefficient γ_i plotted against Co content. These values are also listed in Table I.

entropy S_P^{mag} at $T_{C,P}$ is between 3.3 and 6.6 J mol^{-1} K^{-1}. Thus, as a qualitative consideration, ΔS^{mag} greatly contributes to ΔS^{anom}, which is a key point for the RMT behavior.

The total Gibbs energy change $\Delta G = G_M - G_P$ was calculated and is shown in Fig. 5(b) by using

$$\Delta G = -T\left(\Delta S_0 + \int_0^T \frac{\Delta C_P}{T} dT\right) + \Delta H_0 + \int_0^T \Delta C_P dT,$$
$$\Delta C_P = T\frac{d\Delta S}{dT}, \quad (3)$$

where ΔS is assumed to be given by ΔS_{trend} in Fig. 5(a). ΔS_0 was assumed to be zero, but ΔH_0 was unknown. Therefore, we used $\Delta G = 0$ at $T_{0,HT} = (T_{M_s} + T_{A_f})/2 = 680$ K, which is the case for Co51.7, and ΔG_0 ($= \Delta H_0$) at 0 K was found to be around 170 J mol^{-1}, as indicated in Fig. 5(b). The RMT behavior was obtained with the RMT temperature $T_{0,LT}$ being around 180 K. This value is somewhat reasonable because $T_{0,LT} = (T_{A_f}' + T_{M_s}')/2$ of Co51.6 is 295 K.

D. Specific-heat measurements at low temperatures

In order to obtain further insights into M and P phases, systematic specific-heat measurements on alloys in different phases were performed at low temperatures. The results are shown in Fig. 6(a), where Co48.7, Co49.7, Co50.4, and Co51.3 are in the P phase, while Co53.8, Co54.2, and Co54.9 are in the M phase. The specific heats were found to strongly depend on their phases, rather than their modifications of Co concentration. As shown in the inset of Fig. 6(a), a linear relationship between C_P/T and T^2 holds well. This gives

$$C_{P,i} \approx C_{V,i} = \gamma_i T + \beta_i T^3, \quad (4)$$

where $C_{V,i}$ is the specific heat at constant volume. Conventionally, the first and second terms on the right-hand side of Eq. (4) are considered to be the "electronic" and "lattice" contributions, respectively, in which γ_i is the electronic coefficient and β_i is the lattice coefficient [21]. The apparent Debye temperature is estimated by using

$$\theta_{D,i} = \sqrt[3]{12\pi^4 R/5\beta_i}, \quad (5)$$

where R is the gas constant [21]. $\theta_{D,i}$ and γ_i are summarized in Table I and plotted in Fig. 6(b). This figure also contains the values of $\theta_{D,i}$ and γ_i of Co52.5 with RMT behavior, which were estimated by extrapolating their x dependences to $x = 52.5$.

The obtained values of $\theta_{D,i}$ were found to be large compared with those of NiMn-based Heusler alloys [24]. In addition, $\theta_{D,P}$ generally shows larger values than $\theta_{D,M}$. This behavior is found to be anomalous when their crystal structures are taken into consideration. See Table II for a comparison of θ_D of metals with allotropic transformations. Normally, among the same metals with different structures, the compact phase has a higher θ_D. This originates from the stronger bonding in the compact phases [25]. It can be seen that except for Fe [26], all the elements obey this tendency, and θ_D of the compact phases are higher by 50 to 250 K than those of open phases [21,27–29]. For Fe (bcc), it is believed that because of ferromagnetism, an abnormally greater Debye temperature appears for the bcc phase [25]. As shown in Fig. 6(b), the extrapolation to Co52.5 shows that the $\theta_{D,P}$ (bcc) is higher than $\theta_{D,M}$ (fct) by more than 30 K. Since ferromagnetism also exists in the P phase in Cox alloys, the same reason as that for pure Fe is considered to explain this anomaly. Actually, $\theta_{D,P}$ would be much smaller if

TABLE II. Debye temperatures of pure metals and extrapolated $Co_{52.5}Cr_{25.5}Ga_{11}Si_{11}$ (Co52.5). It can be seen that only Fe and Co52.5 show abnormal behavior, in which the open-structure (bcc) phases have higher Debye temperatures.

Solid	Debye temperature (K)	Reference
Be (bcc)	962–1217 (Calc)	[27]
Be (hcp)	1485	[28]
Cd (bcc)	170	[21]
Cd (hcp)	280	[21]
Ti (bcc)	300	[29]
Ti (hcp)	365	[29]
Sn (bct)	140	[21]
Sn (fcc)	240	[21]
Zr (bcc)	212	[29]
Zr (hcp)	260	[29]
Fe (bcc)	420	[26]
Fe (fcc)	335	[26]
Co52.5 (P, bcc)	414	this work
Co52.5 (M, fct)	381	this work

the P phase were nonmagnetic, which has also been predicted theoretically for ferromagnetic SMAs [30,31].

Moreover, γ_i shows a huge difference between the two phases. The extrapolation to Co52.5 shows that γ_M is about 3 times γ_P, as shown in Fig. 6(b). Specifically, while γ_M has a typical value for transition metallic alloys such as Cu-Mn-Sb [32] and Ni-Fe-Ga [33], γ_P has a typical value for half-metallic alloys [34,35] or strongly spin-polarized alloys [36]. Thus, a drastic change in the electronic state during the RMT is clear.

Finally, we briefly touch upon the entropy derived using Eq. (4). When $C_{P,i}$ given by Eq. (4) with the obtained γ_i and $\theta_{D,i}$ is substituted into Eq. (2), ΔS given by Eq. (1) is shown to be given by the sum of the electronic contribution $\Delta S^{ele} = S_M^{ele} - S_P^{ele}$ and the lattice contribution $\Delta S^{lat} = S_M^{lat} - S_P^{lat}$. $\gamma_M > \gamma_P$ and $\theta_{D,M} < \theta_{D,P}$ observed in Fig. 6(b) give both $\Delta S^{ele} > 0$ and $\Delta S^{lat} > 0$. In this procedure, however, the magnetic contribution to ΔS, ΔS^{mag}, may be overlooked. As was previously discussed, the magnetic system affects the lattice system and considerably changes the Debye temperature. Furthermore, as shown in Fig. 4, the experimental specific heats deviate from those estimated using the Debye model with the experimental values of $\theta_{D,i}$, especially in the case of the paramagnetic M phase. These facts mean that magnetic and lattice freedoms fluctuate thermally and affect each other, and therefore, ΔS_i^{lat} coming from the second term in Eq. (4) should be considered to partly include the magnetic contribution. This also suggests that different sources of entropy can hardly be separated by means of specific-heat measurement when different kinds of phase transition coexist.

IV. CONCLUSIONS

In conclusion, we experimentally investigated the physical properties of $Co_2Cr(Ga,Si)$ shape-memory alloys with ferromagnetic and martensitic transformations. It was found that the electrical resistivity in the parent phase shows an inverse temperature T dependence in contrast to its usual metallic behavior in the martensite phase. We determined the pseudobinary magnetostructural phase diagram, in which a martensite loop region was found, clearly showing the reentrant martensitic transformation behavior. The specific heats and the differential scanning calorimetry were analyzed to obtain the entropy change ΔS between M and P phases, which was confirmed to be consistent with the appearances of both MT and RMT.

ACKNOWLEDGMENTS

This work was supported by Grant-in-Aids for Scientific Research from the Japan Society for the Promotion of Science (JSPS). A part of this work was carried out at the Center for Low Temperature Science, Institute for Materials Research, Tohoku University.

APPENDIX: ROUGH ESTIMATION OF MAGNETIC ENTROPY OF THE CO49.7 ALLOY

We show a rough estimation of the magnetic entropy of the Co49.7 alloy, which is always in the parent phase, by using experimental specific-heat measurements. Several simple assumptions will be made due to insufficient experimental data.

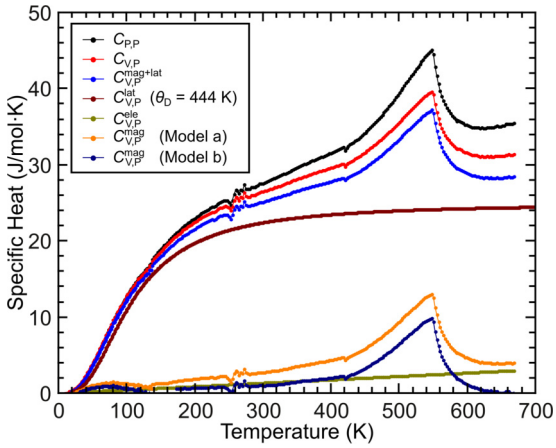

FIG. 7. (Color online) Specific heat under constant pressure ($C_{P,P}$; total specific heat) determined experimentally for the Co49.7 alloy. Specific heats under constant volume ($C_{V,P}$; total specific heat) and of the sum of the magnetic and lattice contributions ($C_{V,P}^{mag+lat}$), magnetic contribution ($C_{V,P}^{mag}$), electronic contribution ($C_{V,P}^{ele}$), and lattice contribution ($C_{V,P}^{lat}$) with a Debye temperature of $\theta_D = 444$ K were also estimated and are shown. Refer to the text for details.

The total specific heat at constant pressure $C_{P,P}$ is shown in Fig. 7, where the data below 137 K were measured using the relaxation method, while those above 137 K were measured using the heat flow method. For the alloy with no MT, the heat capacity under constant volume $C_{V,i}$ is assumed to be presented as

$$C_{V,i} = C_{V,i}^{lat} + C_{V,i}^{ele} + C_{V,i}^{mag}, \tag{A1}$$

where $C_{V,i}^{lat}$, $C_{V,i}^{ele}$, and $C_{V,i}^{mag}$ are the contributions by the lattice, electron (nonmagnetic), and magnetism, respectively. However, before we proceed to separate the components of the specific heat, it is necessary to convert $C_{P,i}$ to $C_{V,i}$. We use the relationship of

$$C_{P,i} - C_{V,i} = V_i T \alpha_i^2 B_i, \tag{A2}$$

where V_i is the molar volume, α_i is the coefficient of volumetric thermal expansion, and B_i is the bulk modulus. For experimental determination of $C_{V,i}$, one has to obtain the temperature dependences of V_i, α_i, and B_i, which are difficult, especially in the case of B_i. Note that these quantities satisfy the empirical relationship

$$C_{P,i} - C_{V,i} = V_i \frac{\alpha_i^2 B_i}{C_{P,i}^2} C_{P,i}^2 T = A_i C_{P,i}^2 T, \tag{A3}$$

where A_i shows little temperature dependence [21]. Therefore, $C_{P,i} - C_{V,i}$ can be obtained only with the knowledge of these quantities at room temperature and the temperature dependence of $C_{P,i}$. Also note that B_i and α_i do not show a large difference as long as the systems are of similar compositions. Hence, for the case of the parent phase, it is possible to calculate A_P by taking the values of $B_P = 190$ GPa and $\alpha_P = 3.75 \times 10^{-5} m^{-3}$ for pure Co [37] and using $V_P = 1.398 \times 10^{-5} m^3/mol$ [1] for the P phase of $Co_{51.5}Cr_{26.5}Ga_{11}Si_{11}$ as a rough estimation. The obtained $C_{V,P}$ is plotted against temperature in Fig. 7. Using this curve, the contribution of the electrons to the specific heat $C_{V,P}^{ele}$ is

subtracted, where

$$C_{\mathrm{V,P}}^{\mathrm{ele}} = \gamma_{\mathrm{P}} T \tag{A4}$$

is assumed. The subtracted curve is shown as $C_{\mathrm{V,P}}^{\mathrm{mag+lat}}$ in Fig. 7. In the first model (model a), the lattice contribution to the specific heat is estimated by assuming the Debye function

$$C_{\mathrm{V,P}}^{\mathrm{lat}} = 9R\left(\frac{T}{\theta_{\mathrm{D,P}}}\right)^3 \int_0^{\theta_{\mathrm{D,P}}/T} \frac{x^4 e^x}{(e^x-1)^2}\, dx. \tag{A5}$$

Equations (A1) and (A3)–(A5) give $C_{\mathrm{V,P}}^{\mathrm{mag}}$, which is shown by the yellow curve (model a) in Fig. 7. $C_{\mathrm{V,P}}^{\mathrm{mag}}$ may be overestimated since $C_{\mathrm{V,P}}^{\mathrm{lat}}$ given by Eq. (A5) is underestimated. As a result, $C_{\mathrm{V,P}}^{\mathrm{mag}}$ remains large at high temperatures, as seen in Fig. 7. In the second model (model b), therefore, $C_{\mathrm{V,P}}^{\mathrm{mag}}$ was adjusted so that it was zero at 650 K by subtracting $C_{\mathrm{V,P}}^{\mathrm{mag}} = 5.77 \times 10^{-3} T$ J mol^{-1} K^{-1} from $C_{\mathrm{V,P}}^{\mathrm{mag}}$ in model a. The resultant $C_{\mathrm{V,P}}^{\mathrm{mag}}$ is shown by the dark blue line (model b) in Fig. 7. Obviously, due to short-range interaction of the spins in the paramagnetic temperature range, $C_{\mathrm{V,P}}^{\mathrm{mag}}$ at 650 K should not be zero, similar to the case of $C_{\mathrm{V}}^{\mathrm{mag}}$ analyzed for pure Fe [38]. Thus, the actual $C_{\mathrm{V,P}}^{\mathrm{mag}}$ might lie between these two limitation models.

In order to obtain the magnetic entropy, $C_{\mathrm{V,P}}^{\mathrm{mag}}$ should be converted back to $C_{\mathrm{P,P}}^{\mathrm{mag}}$ before integration. Putting $C_{\mathrm{V,P}}^{\mathrm{mag}}$ as $C_{\mathrm{V,P}}$ into Eq. (A3) gives

$$C_{\mathrm{P,P}}^{\mathrm{mag}} = \frac{1-\sqrt{1-4A_{\mathrm{P}}TC_{\mathrm{V,P}}^{\mathrm{mag}}}}{2A_{\mathrm{P}}T}, \tag{A6}$$

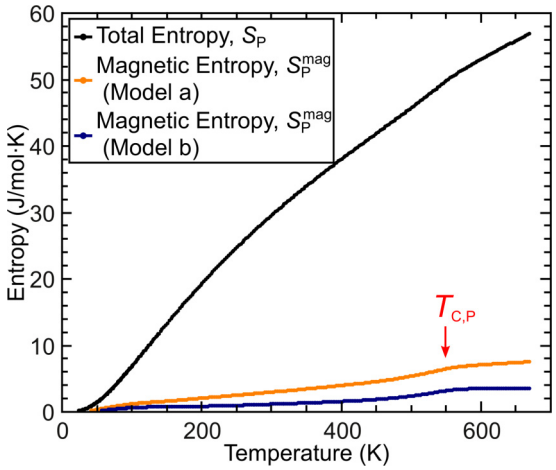

FIG. 8. (Color online) Total entropy and magnetic entropy are plotted for the Co49.7 alloy. Actual values of magnetic entropy are expected to lie between the lines of models a and b.

although the difference between $C_{\mathrm{V,P}}^{\mathrm{mag}}$ and $C_{\mathrm{P,P}}^{\mathrm{mag}}$ is actually very small. Thus, S_{P} and $S_{\mathrm{P}}^{\mathrm{mag}}$ can be obtained using Eq. (2), in which $S_{0,i} = 0$ was assumed. The results are shown in Fig. 8. The actual values of magnetic entropy are expected to lie between the two lines given by models a and b. It can be seen that the magnetic entropy contributes about 6%–13% of the total entropy. Thus, $S_{\mathrm{P}}^{\mathrm{mag}}$ at $T_{\mathrm{C,P}}$ should have a value between 3.3 and 6.6 J mol^{-1} K^{-1}. However, since the phonon softening effect, which is commonly seen in other ferromagnetic shape-memory alloys [39,40], is considered in neither model a nor model b, a noticeable error is expected, and further detailed investigations, such as the temperature dependence of elastic constants, are required.

[1] X. Xu, T. Omori, M. Nagasako, A. Okubo, R. Y. Umetsu, T. Kanomata, K. Ishida, and R. Kainuma, Appl. Phys. Lett. **103**, 164104 (2013).

[2] A. N. Vasil'ev, A. D. Bozhko, V. V. Khovailo, I. E. Dikshtein, V. G. Shavrov, V. D. Buchelnikov, M. Matsumoto, S. Suzuki, T. Takagi, and J. Tani, Phys. Rev. B **59**, 1113 (1999).

[3] W. Ito, K. Ito, R. Y. Umetsu, R. Kainuma, K. Koyama, K. Watanabe, A. Fujita, K. Oikawa, K. Ishida, and T. Kanomata, Appl. Phys. Lett. **92**, 021908 (2008).

[4] Y. Nishino, M. Kato, S. Asano, K. Soda, M. Hayasaki, and U. Mizutani, Phys. Rev. Lett. **79**, 1909 (1997).

[5] J. Barth, G. H. Fecher, B. Balke, S. Ouardi, T. Graf, C. Felser, A. Shkabko, A. Weidenkaff, P. Klaer, H. J. Elmers, H. Yoshikawa, S. Ueda, and K. Kobayashi, Phys. Rev. B **81**, 064404 (2010).

[6] K. U. Neumann, T. Kanomata, B. Ouladdiaf, and K. R. A. Ziebeck, J. Phys.: Condens. Matter **14**, 1371 (2002).

[7] L. Kaufman and M. Cohen, Trans. Am. Inst. Mining Metallurg. Eng. **206**, 1393 (1956).

[8] K. Ullakko, J. K. Huang, C. Kantner, R. C. O'Handley, and V. V. Kokorin, Appl. Phys. Lett. **69**, 1966 (1996).

[9] R. Kainuma, Y. Imano, W. Ito, Y. Sutou, H. Morito, S. Okamoto, O. Kitakami, K. Oikawa, A. Fujita, T. Kanomata, and K. Ishida, Nature (London) **439**, 957 (2006).

[10] R. Y. Umetsu, K. Endo, A. Kondo, K. Kindo, W. Ito, X. Xu, T. Kanomata, and R. Kainuma, Mater. Trans. **54**, 291 (2013).

[11] J. H. Mooij, Phys. Status Solidi A **17**, 521 (1973).

[12] M. Miyakawa, R. Umetsu, K. Fukamichi, H. Yoshida, and E. Matsubara, J. Phys.: Condens. Matter **15**, 4817 (2003).

[13] T. Kasuya, Prog. Theor. Phys. **16**, 58 (1956).

[14] P. G. de Gennes and J. Friedel, J. Phys. Chem. Solids **4**, 71 (1958).

[15] M. Kataoka, Phys. Rev. B **63**, 134435 (2001).

[16] M. Terada, Y. Fujita, and K. Endo, J. Phys. Soc. Jpn. **36**, 620 (1974).

[17] R. Y. Umetsu, R. Kainuma, Y. Amako, Y. Taniguchi, T. Kanomata, K. Fukushima, A. Fujita, K. Oikawa, and K. Ishida, Appl. Phys. Lett. **93**, 042509 (2008).

[18] I. Galanakis, P. H. Dederichs, and N. Papanikolaou, Phys. Rev. B **66**, 174429 (2002).

[19] R. Y. Umetsu, K. Kobayashi, R. Kainuma, A. Fujita, K. Fukamichi, K. Ishida, and A. Sakuma, Appl. Phys. Lett. **85**, 2011 (2004).
[20] R. Y. Umetsu, A. Okubo, X. Xu, and R. Kainuma, J. Alloys Compd. **588**, 153 (2014).
[21] E. S. R. Gopal, *Specific Heats at Low Temperatures* (Plenum, New York, 1966).
[22] P. Wollants, M. De Bonte, and J. Roos, Z. Metallkd. **70**, 113 (1979).
[23] M. Kataoka, T. Kanomata, R. Y. Umetsu, and R. Kainuma, J. Magn. Magn. Mater. **361**, 34 (2014).
[24] V. A. Chernenko, D. V. Homenko, V. A. L'vov, and J. M. Barandiaran, J. Appl. Phys. **109**, 013526 (2011).
[25] R. Smallman and R. Bishop, *Metals and Materials: Science, Processes, Applications* (Butterworth-Heinemann, Oxford, 1995).
[26] R. J. Weiss and K. J. Tauer, Phys. Rev. **102**, 1490 (1956).
[27] K. Kadás, L. Vitos, B. Johansson, and J. Kollár, Phys. Rev. B **75**, 035132 (2007).
[28] C. A. Swenson, J. Appl. Phys. **70**, 3046 (1991).
[29] R. Weiss, *Solid State Physics for Metallurgists* (Pergamon, London, 1963), Vol. 6.
[30] M. A. Uijttewaal, T. Hickel, J. Neugebauer, M. E. Gruner, and P. Entel, Phys. Rev. Lett. **102**, 035702 (2009).
[31] T. Hickel, M. Uijttewaal, A. Al-Zubi, B. Dutta, B. Grabowski, and J. Neugebauer, Adv. Eng. Mater. **14**, 547 (2012).
[32] J. Bœuf, C. Pfleiderer, and A. Faißt, Phys. Rev. B **74**, 024428 (2006).
[33] O. Heczko, S. Fähler, T. M. Vasilchikova, T. N. Voloshok, K. V. Klimov, Y. I. Chumlyakov, and A. N. Vasiliev, Phys. Rev. B **77**, 174402 (2008).
[34] T. Graf, G. H. Fecher, J. Barth, J. Winterlik, and C. Felser, J. Phys. D **42**, 084003 (2009).
[35] R. Y. Umetsu, N. Endo, A. Fujita, A. Kainuma, Rand Sakuma, K. Fukamichi, and K. Ishida, J. Phys. Conf. Ser. **200**, 062036 (2010).
[36] A. N. Vasiliev, O. Heczko, O. S. Volkova, T. N. Vasilchikova, T. N. Voloshok, K. V. Klimov, W. Ito, R. Kainuma, K. Ishida, K. Oikawa, and S. Fähler, J. Phys. D **43**, 055004 (2010).
[37] *Handbook of Metals*, edited by Y. Waseda *et al.* (Maruzen, Tokyo, 1993).
[38] T. Nishizawa, J. Phase Equilib. **16**, 379 (1995).
[39] L. Mañosa, A. Gonzàlez-Comas, E. Obradó, A. Planes, V. A. Chernenko, V. V. Kokorin, and E. Cesari, Phys. Rev. B **55**, 11068 (1997).
[40] A. Planes, E. Obradó, A. Gonzàlez-Comas, and L. Mañosa, Phys. Rev. Lett. **79**, 3926 (1997).